

# The Darkside-20k Data Acquisition System

---

**Fabio Acerbi<sup>1</sup> Pushparaj Adhikari<sup>2</sup> Paolo Agnes<sup>3,4</sup> Iftikhar Ahmad<sup>5</sup> Sebastiano Albergo<sup>6,7</sup>  
 Ivone F.M. Albuquerque<sup>8</sup> Thomas Olling Alexander<sup>9</sup> Andrew Knight Alton<sup>10</sup> Pierre-André  
 Amaudruz<sup>11</sup> Gioacchino Alex Anastasi<sup>6,7</sup> Michele Angiolilli<sup>4,3</sup> Elena Aprile<sup>12</sup> David J.  
 Auty<sup>13</sup> Maximo Ave Pernas<sup>3</sup> Oscar Azzolini<sup>14</sup> Henning Olling Back<sup>9</sup> Zoe Balmforth<sup>15</sup> Ana  
 Isabel Barrado Olmedo<sup>16</sup> Pierre Barrillon<sup>17</sup> Giovanni Batignani<sup>18,19</sup> Swadheen Bharat<sup>20</sup>  
 Pritindra Bhowmick<sup>21</sup> Sofia Blua<sup>22,23</sup> Valerio Bocci<sup>24</sup> Walter Bonivento<sup>25</sup> Bianca  
 Bottino<sup>26,27</sup> Mark G. Boulay<sup>2</sup> Titanilla Braun<sup>21</sup> Andrzej Buchowicz<sup>28</sup> Severino  
 Bussino<sup>29,30</sup> José Busto<sup>17</sup> Matteo Cadeddu<sup>25</sup> Mariano Cadoni<sup>25</sup> Roberta Calabrese<sup>31,32</sup>  
 Vincenzo Camillo<sup>33</sup> Alessio Caminata<sup>27</sup> Nicola Canci<sup>31</sup> Andrea Capra<sup>11</sup> Mauro Caravati<sup>25</sup>  
 Miguel Cárdenas-Montes<sup>16</sup> Nicola Cargioli<sup>25</sup> Marco Carlini<sup>4</sup> Paolo Castello<sup>25</sup> Paolo  
 Cavalcante<sup>4</sup> Susana Cebrian<sup>20</sup> Alexander Chepurinov<sup>74</sup> Sarthak Choudhary<sup>34</sup> Luisa  
 Cifarelli<sup>35,36</sup> Yann Coadou<sup>17</sup> Iván Coarasa<sup>20</sup> Valentina Cocco<sup>25</sup> Estefania Conde Vilda<sup>16</sup>  
 Lucia Consiglio<sup>4</sup> Harrison Coombes<sup>33</sup> André Filipe Ventura Cortez<sup>34</sup> Barbara S. Costa<sup>8</sup>  
 Milena Czubak<sup>37</sup> Saverio D'Auria<sup>38,39</sup> Manuel Dionisio Da Rocha Rolo<sup>22</sup> Alexander  
 Dainty<sup>40</sup> Giovanni Darbo<sup>27</sup> Stefano Davini<sup>27</sup> Riccardo de Asmundis<sup>31</sup> Sandro De  
 Cecco<sup>41,24</sup> Marzio De Napoli<sup>6,7</sup> Giulio Dellacasa<sup>22</sup> Alexander Derbin<sup>74</sup> Lea Di Noto<sup>27,26</sup>  
 Philippe Di Stefano<sup>42</sup> Daniel Díaz Mairena<sup>16</sup> Carlo Dionisi<sup>41,24</sup> Grigory Dolganov<sup>74</sup>  
 Francesca Dordei<sup>25</sup> Aaron Elersich<sup>43</sup> Emma Ellingwood<sup>44</sup> Tyler Erjavec<sup>43</sup> Niamh  
 Fearon<sup>21</sup> Marta Fernandez Diaz<sup>16</sup> Luca Ferro<sup>25,45</sup> Andrea Ficarella<sup>1</sup> Giuliana Fiorillo<sup>32,31</sup>  
 Dylan Fleming<sup>43</sup> Paolo Franchini<sup>21</sup> Davide Franco<sup>46</sup> Heriques Frandini Gatti<sup>47</sup> Federico  
 Gabriele<sup>25</sup> Devidutta Gahan<sup>4</sup> Cristiano Galbiati<sup>48</sup> Grzegorz Galiński<sup>28</sup> Giacomo Gallina<sup>48</sup>  
 Marco Garbini<sup>36,49</sup> Pablo Garcia Abia<sup>16</sup> Andrzej Gawdzik<sup>50</sup> Graham Kurt Giovanetti<sup>51</sup>  
 Alberto Gola<sup>1</sup> Luca Grandi<sup>52</sup> Gianfrancesco Grauso<sup>31</sup> Giovanni Grilli di Cortona<sup>4</sup> Alexey  
 Grobov<sup>74</sup> Maxim Gromov<sup>74</sup> Julián Guerrero Cánovas<sup>16</sup> Marisa Gulino<sup>53,54</sup> Samuel  
 Belayneh Habtemariam<sup>34</sup> Brianna Rae Hackett<sup>9</sup> Aksel Hallin<sup>13</sup> Malgorzata Haranczyk<sup>37</sup>  
 Timothée Hessel<sup>46</sup> Celin Hidalgo<sup>3</sup> James Hollingham<sup>40</sup> Sosuke Horikawa<sup>55</sup> Jie Hu<sup>13</sup>  
 Fabrice Hubaut<sup>17</sup> Daniel Huff<sup>56</sup> Théo Hugues<sup>42</sup> Andrea Ianni<sup>48</sup> Valerio Ippolito<sup>24</sup> Ako  
 Jamil<sup>48</sup> Chris Jillings<sup>57,58</sup> Rijeesh Keloth<sup>33</sup> Níkolos Kemmerich<sup>8</sup> Ashlea Kemp<sup>40</sup> Kaori  
 Kondo<sup>4,59</sup> George Korga<sup>21</sup> Lucy Kotsiopoulou<sup>44</sup> Seraphim Koulosousas<sup>60</sup> Pablo Kunzé<sup>3</sup>  
 Michael Kuss<sup>18</sup> Marcin Kuźniak<sup>34</sup> Maciej Kuzwa<sup>34</sup> Marco La Commara<sup>61,31</sup> Michela Lai<sup>42</sup>  
 Emmanuel Le Guirriec<sup>17</sup> Elizabeth Leason<sup>21</sup> Alfiero Leoni<sup>4,59</sup> Lance Lidey<sup>9</sup> John D Lipp<sup>40</sup>  
 Marcello Lissia<sup>25</sup> Ludovico Luzzi<sup>43</sup> Olga Lychagina<sup>43</sup> Oliver Macfadyen<sup>51</sup> Janna Machts<sup>46</sup>  
 Igor Machulin<sup>74</sup> Szymon Manecki<sup>57,58</sup> Ioannis Manthos<sup>15</sup> Andrea Marasciulli<sup>4</sup> Stefano  
 Maria Mari<sup>29,30</sup> Camillo Mariani<sup>33</sup> Jelena Maricic<sup>55</sup> Maria Martinez<sup>20</sup> Giuseppe  
 Matteucci<sup>32,31</sup> Konstantinos Mavrokoridis<sup>47</sup> Arthur B. McDonald<sup>42</sup> Luo Meng<sup>52</sup> Stefano  
 Merzi<sup>1</sup> Andrea Messina<sup>41</sup> Radovan Milincic<sup>55</sup> Graham Miller<sup>50</sup> Saverio Minutoli<sup>27</sup> Ankush**

**Mitra<sup>62</sup> Jocelyn Monroe<sup>21</sup> Matteo Morrocchi<sup>18</sup> Abdulrahman Morsy<sup>63</sup> Valentina Muratova<sup>74</sup> Michael Murra<sup>12</sup> Carlo Muscas<sup>25,64</sup> Paolo Musico<sup>27</sup> Rosario Nania<sup>36</sup> Marzio Nessi<sup>65</sup> Grzegorz Nieradka<sup>34</sup> Konstantinos Nikolopoulos<sup>66</sup> Evangelia Nikoloudaki<sup>46</sup> Jaroslaw Nowak<sup>67</sup> Konstantin Olchanski<sup>11</sup> Andrey Oleinik<sup>74</sup> Paolo Organtini<sup>4,48</sup> Alfonso Ortiz de Solórzano<sup>20</sup> Anantha Padmanabhan<sup>42</sup> Marco Pallavicini<sup>26,27</sup> Luciano Pandola<sup>53</sup> Emilija Pantic<sup>43</sup> Eugenio Paoloni<sup>18,19</sup> Danial Papi<sup>13</sup> Byungju Park<sup>13</sup> Grzegorz Pastuszek<sup>28</sup> Giovanni Paternoster<sup>1</sup> Riccardo Pavarani<sup>25,45</sup> Alec Peck<sup>5</sup> Paolo Attilio Pegoraro<sup>25,64</sup> Krzysztof Pelczar<sup>37</sup> Ramon Perez<sup>8</sup> Vicente Pesudo<sup>16</sup> Stefano Piacentini<sup>3</sup> Noemi Pino<sup>53</sup> Guillaume Plante<sup>12</sup> Andrea Pietro Pocar<sup>63</sup> Stephen Pordes<sup>33</sup> Pascal Pralavorio<sup>17</sup> Elettra Preosti<sup>48</sup> Darren Price<sup>50</sup> George Prior<sup>21</sup> Manuel Pronesti<sup>17</sup> Sebastiana Puglia<sup>6,7</sup> Maria Cecilia Queiroga Bazetto<sup>47</sup> Fabrizio Raffaelli<sup>18</sup> Francesco Ragusa<sup>38</sup> Yorck Ramachers<sup>62</sup> Alejandro Ramirez<sup>56</sup> Sudikshan Ravinthiran<sup>47</sup> Marco Razeti<sup>25</sup> Andrew Lee Renshaw<sup>56</sup> Aras Repond<sup>5</sup> Marco Rescigno<sup>24</sup> Silvia Resconi<sup>39</sup> Fabrice Retiere<sup>11</sup> Ash Ritchie-Yates<sup>50</sup> Angelo Rivetti<sup>22</sup> Adam Roberts<sup>47</sup> Conner Roberts<sup>50</sup> Diego Rodríguez Rodas<sup>34</sup> Giovanni Rogers<sup>66</sup> Luciano Romero<sup>16</sup> Matteo Rossi<sup>26</sup> Dmitry Rudik<sup>32,31</sup> James Runge<sup>63</sup> Maria Adriana Sabia<sup>24</sup> Camilla Salerno<sup>3</sup> Paolo Salomone<sup>24,52</sup> Simone Sanfilippo<sup>53</sup> Daria Santone<sup>21</sup> Roberto Santorelli<sup>16</sup> Edivaldo M. Santos<sup>8</sup> Isobel Sargeant<sup>40</sup> María Luisa Sarsa<sup>20</sup> Claudio Savarese<sup>68</sup> Eugenio Scapparone<sup>36</sup> Fred Schuckman<sup>42</sup> Dmitriy Semenov<sup>74</sup> Carmen Seoane<sup>20</sup> Michela Sestu<sup>25,45</sup> Veronika Shalamova<sup>5</sup> Sanjay Sharma Poudel<sup>56</sup> Marino Simeone<sup>69</sup> Peter Skensved<sup>42</sup> Mikhail Skorokhvatov<sup>74</sup> Taisiia Smirnova<sup>5</sup> Ben Smith<sup>11</sup> Robert Smith<sup>39</sup> Franco Spadoni<sup>9</sup> Martin Spangenberg<sup>62</sup> Arianna Steri<sup>25</sup> Vincenzo Stornelli<sup>4,59</sup> Simone Stracka<sup>18</sup> Allan Sung<sup>48</sup> Clea Sunny<sup>34</sup> Yury Suvorov<sup>32,31</sup> Andrzej M Szelc<sup>44</sup> Oscar Taborda<sup>3</sup> Benjamin Tam<sup>21</sup> Roberto Tartaglia<sup>4</sup> Alan Taylor<sup>47</sup> Jonathan Taylor<sup>47</sup> Gemma Testera<sup>27</sup> Kevin Thieme<sup>55</sup> Angus Thompson<sup>60</sup> Sebastian Torres-Lara<sup>56</sup> Alessia Tricomi<sup>6,7</sup> Sara Tullio<sup>25,45</sup> Evgeniy Unzhakov<sup>74</sup> Marie Van Uffelen<sup>21</sup> Pedro Ventura<sup>8</sup> Guillermo Vera Díaz<sup>16</sup> Simon Viel<sup>2</sup> Alina Vishneva<sup>74</sup> Bruce Vogelaar<sup>33</sup> Joost Vossebeld<sup>47</sup> Bansari Vyas<sup>2</sup> Masayuki Wada<sup>34</sup> Marek Bohdan Walczak<sup>3</sup> Yi Wang<sup>70,71</sup> Shawn Westerdale<sup>5</sup> Laurie Williams<sup>72</sup> Marcin Marian Wojcik<sup>37</sup> Mariusz Wojcik<sup>73</sup> Changgen Yang<sup>70,71</sup> Jilong Yin<sup>70,71</sup> Azam Zabihi<sup>34</sup> Paul Zakhary<sup>7,6</sup> Andrea Zani<sup>39</sup> Haoxiang Zhan<sup>50</sup> Yongpeng Zhang<sup>70,71</sup> Antonino Zichichi<sup>†35,36</sup> Grzegorz Zuzel<sup>37</sup>**

<sup>1</sup> *Fondazione Bruno Kessler, Povo, 38123, Italy*

<sup>2</sup> *Department of Physics, Carleton University, Ottawa, ON K1S 5B6, Canada*

<sup>3</sup> *Gran Sasso Science Institute, L'Aquila, 67100, Italy*

<sup>4</sup> *INFN Laboratori Nazionali del Gran Sasso, Assergi (AQ), 67100, Italy*

<sup>5</sup> *Center for Experimental Cosmology & Instrumentation, Riverside, CA 92507, USA*

<sup>6</sup> *INFN Catania, Catania, 95121, Italy*

<sup>7</sup> *Università of Catania, Catania, 95124, Italy*

<sup>8</sup> *Instituto de Física, Universidade de São Paulo, São Paulo, 05508-090, Brazil*

<sup>9</sup> *Pacific Northwest National Laboratory, Richland, WA 99352, USA*

<sup>10</sup> *Physics Department, Augustana University, Sioux Falls, SD 57197, USA*

<sup>11</sup> *TRIUMF, 4004 Wesbrook Mall, Vancouver, BC V6T 2A3, Canada*

<sup>12</sup> *Physics Department, Columbia University, New York, NY 10027, USA*

<sup>13</sup> *Department of Physics, University of Alberta, Edmonton, AB T6G 2R3, Canada*

- <sup>14</sup>*INFN Laboratori Nazionali di Legnaro, Legnaro (Padova), 35020, Italy*
- <sup>15</sup>*Institute for Experimental Physics, University of Hamburg, Hamburg, 22761, Germany*
- <sup>16</sup>*CIEMAT, Centro de Investigaciones Energéticas, Medioambientales y Tecnológicas, Madrid, 28040, Spain*
- <sup>17</sup>*Centre de Physique des Particules de Marseille, Aix Marseille Univ, CNRS/IN2P3, CPPM, Marseille, France*
- <sup>18</sup>*INFN Pisa, Pisa, 56127, Italy*
- <sup>19</sup>*Physics Department, Università degli Studi di Pisa, Pisa, 56127, Italy*
- <sup>20</sup>*Centro de Astropartículas y Física de Altas Energías, Universidad de Zaragoza, Zaragoza, 50009, Spain*
- <sup>21</sup>*Department of Physics, University of Oxford, Oxford, OX1 3RH, UK*
- <sup>22</sup>*INFN Torino, Torino, 10125, Italy*
- <sup>23</sup>*Department of Electronics and Communications, Politecnico di Torino, Torino, 10129, Italy*
- <sup>24</sup>*INFN Sezione di Roma, Roma, 00185, Italy*
- <sup>25</sup>*INFN Cagliari, Cagliari, 09042, Italy*
- <sup>26</sup>*Physics Department, Università degli Studi di Genova, Genova, 16146, Italy*
- <sup>27</sup>*INFN Genova, Genova, 16146, Italy*
- <sup>28</sup>*Warsaw University of Technology, Warsaw, 00-661, Poland*
- <sup>29</sup>*INFN Roma Tre, Roma, 00146, Italy*
- <sup>30</sup>*Mathematics and Physics Department, Università degli Studi Roma Tre, Roma, 00146, Italy*
- <sup>31</sup>*INFN Napoli, Napoli, 80126, Italy*
- <sup>32</sup>*Physics Department, Università degli Studi “Federico II” di Napoli, Napoli, 80126, Italy*
- <sup>33</sup>*Virginia Tech, Blacksburg, VA 24061, USA*
- <sup>34</sup>*AstroCeNT, Nicolaus Copernicus Astronomical Center of the Polish Academy of Sciences, Warsaw, 00-614, Poland*
- <sup>35</sup>*Department of Physics and Astronomy, Università degli Studi di Bologna, Bologna, 40126, Italy*
- <sup>36</sup>*INFN Bologna, Bologna, 40126, Italy*
- <sup>37</sup>*M. Smoluchowski Institute of Physics, Jagiellonian University, Krakow, 30-348, Poland*
- <sup>38</sup>*Physics Department, Università degli Studi di Milano, Milano, 20133, Italy*
- <sup>39</sup>*INFN Milano, Milano, 20133, Italy*
- <sup>40</sup>*Science & Technology Facilities Council (STFC), Rutherford Appleton Laboratory, Technology, Harwell Oxford, Didcot, OX11 0QX, UK*
- <sup>41</sup>*Physics Department, Sapienza Università di Roma, Roma, 00185, Italy*
- <sup>42</sup>*Department of Physics, Engineering Physics and Astronomy, Queen’s University, Kingston, ON K7L 3N6, Canada*
- <sup>43</sup>*Department of Physics, University of California Davis, Davis, CA 95616, USA*
- <sup>44</sup>*School of Physics and Astronomy, University of Edinburgh, Edinburgh, EH9 3FD, UK*
- <sup>45</sup>*Physics Department, Università degli Studi di Cagliari, Cagliari, 09042, Italy*
- <sup>46</sup>*APC, Université de Paris, CNRS, Astroparticule et Cosmologie, Paris, F-75013, France*
- <sup>47</sup>*Department of Physics, University of Liverpool, The Oliver Lodge Laboratory, Liverpool, L69 7ZE, UK*
- <sup>48</sup>*Physics Department, Princeton University, Princeton, NJ 08544, USA*
- <sup>49</sup>*Museo Storico della Fisica e Centro Studi e Ricerche Enrico Fermi, Roma, 00184, Italy*
- <sup>50</sup>*Department of Physics and Astronomy, The University of Manchester, Manchester, M13 9PL, UK*
- <sup>51</sup>*Williams College, Department of Physics and Astronomy, Williamstown, MA 01267, USA*
- <sup>52</sup>*Department of Physics and Kavli Institute for Cosmological Physics, University of Chicago, Chicago, IL 60637, USA*

- <sup>53</sup>*INFN Laboratori Nazionali del Sud, Catania, 95123, Italy*
- <sup>54</sup>*Engineering and Architecture Department, Università di Enna Kore, Enna, 94100, Italy*
- <sup>55</sup>*Department of Physics and Astronomy, University of Hawai'i, Honolulu, HI 96822, USA*
- <sup>56</sup>*Department of Physics, University of Houston, Houston, TX 77204, USA*
- <sup>57</sup>*Department of Physics and Astronomy, Laurentian University, Sudbury, ON P3E 2C6, Canada*
- <sup>58</sup>*SNOLAB, Lively, ON P3Y 1N2, Canada*
- <sup>59</sup>*Università degli Studi dell'Aquila, L'Aquila, 67100, Italy*
- <sup>60</sup>*Department of Physics, Royal Holloway University of London, Egham, TW20 0EX, UK*
- <sup>61</sup>*Pharmacy Department, Università degli Studi "Federico II" di Napoli, Napoli, 80131, Italy*
- <sup>62</sup>*University of Warwick, Department of Physics, Coventry, CV47AL, UK*
- <sup>63</sup>*Amherst Center for Fundamental Interactions and Physics Department, University of Massachusetts, Amherst, MA 01003, USA*
- <sup>64</sup>*Department of Electrical and Electronic Engineering, Università degli Studi di Cagliari, Cagliari, 09123, Italy*
- <sup>65</sup>*Istituto Nazionale di Fisica Nucleare, Roma, 00186, Italia*
- <sup>66</sup>*School of Physics and Astronomy, University of Birmingham, Edgbaston, Birmingham, B15 2TT, UK*
- <sup>67</sup>*Physics Department, Lancaster University, Lancaster, LA1 4YB, UK*
- <sup>68</sup>*Center for Experimental Nuclear Physics and Astrophysics, and Department of Physics, University of Washington, Seattle, WA 98195, USA*<sup>instit</sup>
- <sup>69</sup>*Chemical, Materials, and Industrial Production Engineering Department, Università degli Studi "Federico II" di Napoli, Napoli, 80126, Italy*
- <sup>70</sup>*Institute of High Energy Physics, Beijing, 100049, China*
- <sup>71</sup>*University of Chinese Academy of Sciences, Beijing, 100049, China*
- <sup>72</sup>*Department of Physics and Engineering, Fort Lewis College, Durango, CO 81301, USA*
- <sup>73</sup>*Institute of Applied Radiation Chemistry, Lodz University of Technology, Lodz, 93-590, Poland*
- <sup>74</sup>*ORCID 0000-0002-1767-1754, ORCID 0000-0002-4351-2255, ORCID 0000-0002-6394-9219, ORCID 0000-0002-8468-9540, ORCID 0000-0003-2869-2363, ORCID 0009-0009-0770-8830, ORCID 0000-0002-0597-2234, ORCID 0000-0001-5532-7711, ORCID 0000-0002-1455-4341, ORCID 0009-0005-0286-0156, ORCID 0000-0002-5527-4880, ORCID 0000-0003-2952-6412, ORCID 0000-0002-2624-9416*
- <sup>†</sup>*Deceased*

*E-mail: ds-ed@lists.infn.it*

**ABSTRACT:** DarkSide-20k is a Weakly Interacting Massive Particles (WIMP) search experiment using liquid argon as a target, designed to perform a background-free search for dark matter with unprecedented sensitivity, and is currently under construction at INFN Laboratori Nazionali del Gran Sasso, Italy. The detector comprises a dual-phase Time Projection Chamber complemented with external veto systems and is equipped with a total of 2720 Silicon PhotoMultiplier (SiPM)-based readout channels. This work presents the Data Acquisition (DAQ) system designed for DarkSide-20k. The system is capable of continuous, triggerless digitisation of the waveforms with high single-photoelectron detection efficiency and online processing, ensuring data reduction for long-term storage.

The DarkSide-20k DAQ system employs commercial CAEN VX2745 digitisers with custom FPGA firmware implementation. Timing and synchronisation across all 48 digitisers are provided by custom Global and Crate Data Manager boards distributing a phase-aligned clock derived from a disciplined rubidium standard. Waveform segments are processed in real time by Front End Processor machines. Data are organised into collections containing whole detector information and distributed across a farm of Time Slice Processors for event reconstruction, classification, and further reduction before storage and offline analysis.

A full “Quadrant” of the system, corresponding to one quarter of the final DAQ, has been assembled and validated at TRIUMF laboratory in Canada. The Quadrant has been stress-tested with simultaneous pulses and demonstrated sustained digitizer readout exceeding expected physics rates and stable long-term performance.

**KEYWORDS:** Data Acquisition (DAQ), Front-end electronics for detector readout, Online farms, online filtering, Dark Matter detector, Time Projection Chamber (TPC)

---

## Contents

<b>1</b>	<b>Introduction</b>	<b>1</b>
<b>2</b>	<b>DAQ architecture</b>	<b>4</b>
2.1	DAQ infrastructure	6
<b>3</b>	<b>Time Slice Concept</b>	<b>6</b>
<b>4</b>	<b>Waveform Digitisation and Filtering</b>	<b>7</b>
<b>5</b>	<b>Global Data Manager and Crate Data Manager</b>	<b>11</b>
<b>6</b>	<b>Front End Processors</b>	<b>14</b>
<b>7</b>	<b>Data Flow Control, Pool Manager (PM) and Midas supervisor</b>	<b>15</b>
<b>8</b>	<b>Time Slice Processors and Merger</b>	<b>17</b>
<b>9</b>	<b>Slow Control</b>	<b>18</b>
<b>10</b>	<b>Quadrant Test</b>	<b>19</b>
<b>11</b>	<b>Conclusions</b>	<b>20</b>

---

## 1 Introduction

This paper describes the DAQ system of the DarkSide-20k (DS-20k) experiment. DS-20k is a next-generation, multi-tonne Dark Matter (DM) detector under construction at the INFN Laboratori Nazionali del Gran Sasso (LNGS). Designed to achieve leading sensitivity in the search for WIMPs over the next decade, DS-20k will probe the DM mass range from  $1 \text{ GeV}c^2$  to  $10 \text{ TeV}c^2$  via Nuclear Recoil (NR). The experiment is designed to reach the sensitivity level where solar and atmospheric neutrinos become significant backgrounds [1, 2].

The core detection system of DS-20k is a dual-phase Time Projection Chamber (TPC) with a vertical electron drift field (see Figure 1). The TPC is a 348 cm tall octagonal prism made of transparent acrylic with a 350 cm inner diameter, containing 50 tonnes of liquid argon extracted from underground sources, that acts as a DM target [1].

The TPC is instrumented with two arrays of SiPM-based photosensors, organised into 2112 readout channels. These arrays, called Optical Planes, are placed on the top and bottom of the TPC and provide an optical coverage of  $21 \text{ m}^2$ . SiPMs are assembled in  $49.5 \times 49.5 \text{ mm}^2$  modules referred to as *Tiles*. Signals from the Tiles are amplified, shaped, and summed by cryogenic low-noise readout electronics, and delivered as a differential signal to Waveform Digitisers

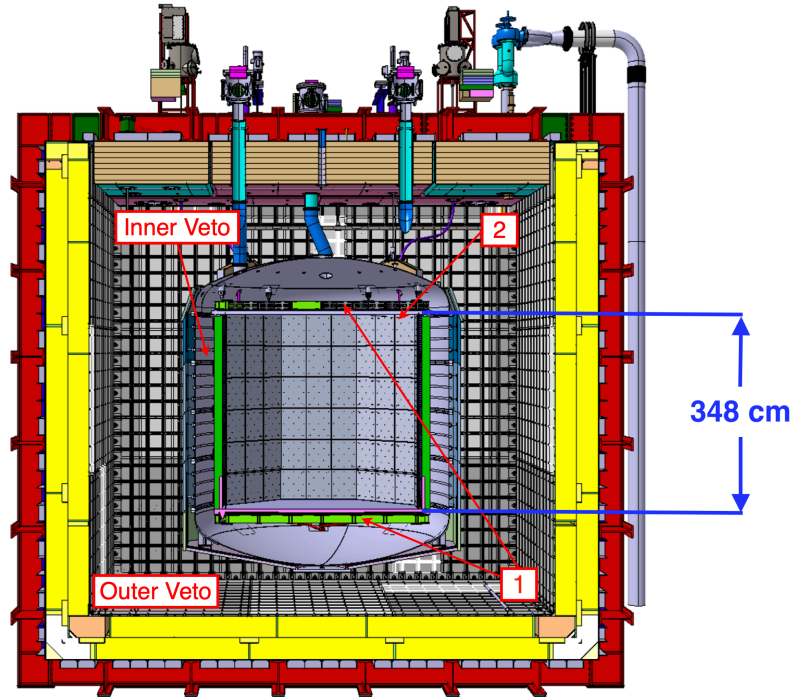


**Figure 1.** Cross-sectional view of the DS-20k detector. The TPC is equipped with top and bottom Optical Planes (1). At the top of the TPC (2), a thin layer of gaseous argon together with a stainless-steel grid enables the production of the electroluminescence signal. The TPC is enclosed in the Inner and Outer Vetos (IV and OV).

(WFDs) operating at room temperature outside of the cryostat. A readout channel is made by the analogue sum of the signals from four Tiles [3, 4]. Four channels (i.e. 16 Tiles) are hosted on a mechanically independent unit of size  $20 \times 20 \text{ cm}^2$  known as Photon Detection Units (PDUs). Single photo-electron signals from one channel exhibit, at the digitiser level and under typical operating conditions, a 14 mV amplitude with a signal to noise ratio of about 6, a rise time of approximately 100 ns, and an exponential decay of about 300 ns.

The TPC Optical Planes detect the prompt scintillation signal (S1) produced by an interaction in liquid argon and the secondary signal (S2) from electroluminescence by the ionisation electrons as they pass through the gas layer below the anode [5].

Electric fields inside the TPC are defined by three electrodes: the cathode on the inner face of the bottom cap of the TPC, the anode on the inner face of the top cap of the TPC, and a grid of wires covering the cross section of the TPC positioned 1 cm below the anode. During standard operation, the grid is immersed 3 mm below the liquid argon surface. Above the surface, a 7 mm thick layer of gaseous argon separates the liquid from the anode. The drift field (typically  $200 \text{ V cm}^{-1}$ ) is established between the cathode and the wire-grid and is responsible for transporting the ionization electrons produced by particle interactions in the liquid argon toward the liquid–gas interface. The extraction field (typically  $5 \text{ kV cm}^{-1}$ ), established between the wire-grid and the anode, enables the efficient extraction of these electrons from the liquid into the gas phase and accelerates them toward the anode, where they generate proportional scintillation light. Graded field rings are used on the

inner walls of the TPC to ensure a uniform field in the drift volume. The cathode, anode and field ring electrodes are made using Clevios<sup>™</sup>, a transparent conductive coating. An arrangement of high-efficiency reflectors cover the inner walls of the TPC. The reflectors, the anode and the cathode are coated with TetraPhenyl Butadiene (TPB) wavelength shifter to convert the argon scintillation (in the VUV) to the sensitive range of the SiPMs [6].

The TPC is surrounded by a stainless steel vessel containing an additional 36 tonnes of underground argon, forming the Inner Veto (IV). This vessel is further immersed in 650 tonnes of liquefied atmospheric argon within a DUNE-like membrane cryostat, serving as the Outer Veto (OV) [7]. Both veto systems are instrumented with SiPM-based photosensors to collect the scintillation light: 480 and 128 channels for the IV and OV, respectively [8]. The IV enables efficient neutron tagging, which is critical since neutrons can mimic DM interactions in the TPC. The OV provides additional passive shield against external neutrons and acts as an active cosmic muon veto.

The DS-20k DAQ is designed to continuously acquire signals from the TPC and Veto photosensors. Analogue waveforms are digitised and transferred to the next stage for processing without waiting for a trigger decision. In this sense, the DS-20k experiment operates in *triggerless mode*, where the data stream is uninterrupted, and the isolation of interesting signals for physics searches is offloaded to an online computing farm (section 3). This architecture is engineered to avoid biases from any specific trigger configuration and decisions based on incomplete detector information, enabling the search for a wide range of dark matter and astrophysical signals, like supernova neutrino bursts. The design of the DAQ system must satisfy stringent performance requirements: (i) ensure a sensitivity to single photoelectrons with an efficiency greater than 90%; (ii) handle an input event rate of approximately 100 events per second in the TPC, increasing up to 200 events per second during calibration runs; and (iii) reducing the data volume from about 3 GB/s at the digitizer level to the projected 60 MB/s on permanent storage during standard operations, and below 200 MB/s during calibration.

The expected event rate in the Inner Detector (TPC and IV) is of the order of 200 events per second. The S1 signals in the energy range relevant for DM searches consist of about 100 photo-electrons spread rather uniformly over the photo-sensor planes. Because of the large number of readout channels, the signal of interest consists mainly of single photo-electrons. This allows for a significant data reduction if parameters such as pulse charge, timing, and prominence (peak amplitude over the baseline) can be computed online. At higher energies, S1 signals are still characterised by relatively short pulses, thus posing little burden to the DAQ system.

The typical S2 signal is of the order of thousands of PEs, a factor of 10, or more, larger than its accompanying S1. The primary challenge for the DAQ system arises from the high data rate generated by the S2 light in the TPC. Typically, only 25% of the light is concentrated in a 3x3 readout channel matrix immediately above the position of the interaction in the  $x - y$  plane. The remaining light is sparse over all the TPC channels, including the bottom plane. Due to substantial amplification of the S2 signal in the gas phase a high number of channels need to be read with long acquisition windows simultaneously. This constitutes a challenge for the data acquisition. The high event rate expected in the OV requires the implementation of less stringent requirements in terms of single photo-electron efficiency and timing resolution, the details of which are still under development.

## 2 DAQ architecture

Figure 2 presents a schematic overview of the DS-20k DAQ system and the network that interconnects its components. The lower part of the diagram shows the hardware elements installed on top of the cryostat, while the upper part presents the elements located in the IT room near the detector. Starting from the bottom of the diagram, the custom-built Global Data Manager (GDM, 1) and Crate Data Manager (CDMs, 2) boards are shown. These boards are interconnected and distribute clock and command signals to the WFDs serving the veto systems (blue and green, 3) and the TPC channels (red, 4) (see section 5).

Each digitiser is connected through a network switch (5) to dedicated Front End Processor computers (FEP, 6), where individual digitised waveforms are processed in software to identify peaks, or *hits*, and extract relevant signal information (see section 6).

WFDs are connected to the switch via 10 Gigabit Ethernet (10 GbE) Direct Attach Cables, while optical Multi-mode cables connect the WFD network switches to the FEPs, which are in turn connected to the main data switches (7) via 10 GbE Direct Attach Cables.

The maximum data output rate of each WFD is dictated by the speed of its network interface, which can use 10 Gbps standard, far exceeding the experiment's needs. The system has been tested to run sustainably at 250 MB/s per digitiser, with the main limitation being the FEPs data processing (see section 10).

To optimise data flow in the DS-20k DAQ system, WFDs employ onboard digital filtering and a time-over-threshold algorithm to identify interesting waveform segments. Only waveform segments containing at least one photoelectron are transmitted to the FEPs. This process, managed by the FPGA-based Dynamic Acquisition Window algorithm, efficiently discards waveform samples lacking relevant physics information, significantly reducing data volume without compromising signal integrity. Monte Carlo simulations indicate that the aggregate expected data rate from a single digitiser for the TPC has a strong dependence on the actual dark count rate of the photosensors. Assuming a dark rate of 400 Hz per channel, a factor 10 in excess of what has been measured in vacuum with pre-production SiPMs, the simulation predicts about 60 MB/s per board, comfortably within the rate mentioned above. Additional compression techniques and/or waveform downsampling in firmware can provide further data reduction if needed.

Next the data are transferred to the FEP, where waveforms are processed and only the time, charge and prominence of the hits identified within the waveform are retained. This approach minimises data volume while preserving necessary event information for offline analyses. Full waveforms can be additionally saved for debugging purposes if needed.

From the data switches, data are distributed via Direct Attach Cables to a cluster of Time Slice Processors (TSPs, 9), where the entire detector data from a predefined time period (Time Slices, see section 3) are merged and where online reconstruction is performed, enabling further data reduction.

The Time Slices from multiple TSPs are collected by the Merger machine (10) and stored on disk (see section 8). The data stream can be delivered to an additional, dedicated machine that performs online processing of pre-selected data fragments for a combined physics analysis across all subdetectors, possibly contributing to the Supernova Early Warning System (SNEWS 2.0) [9].

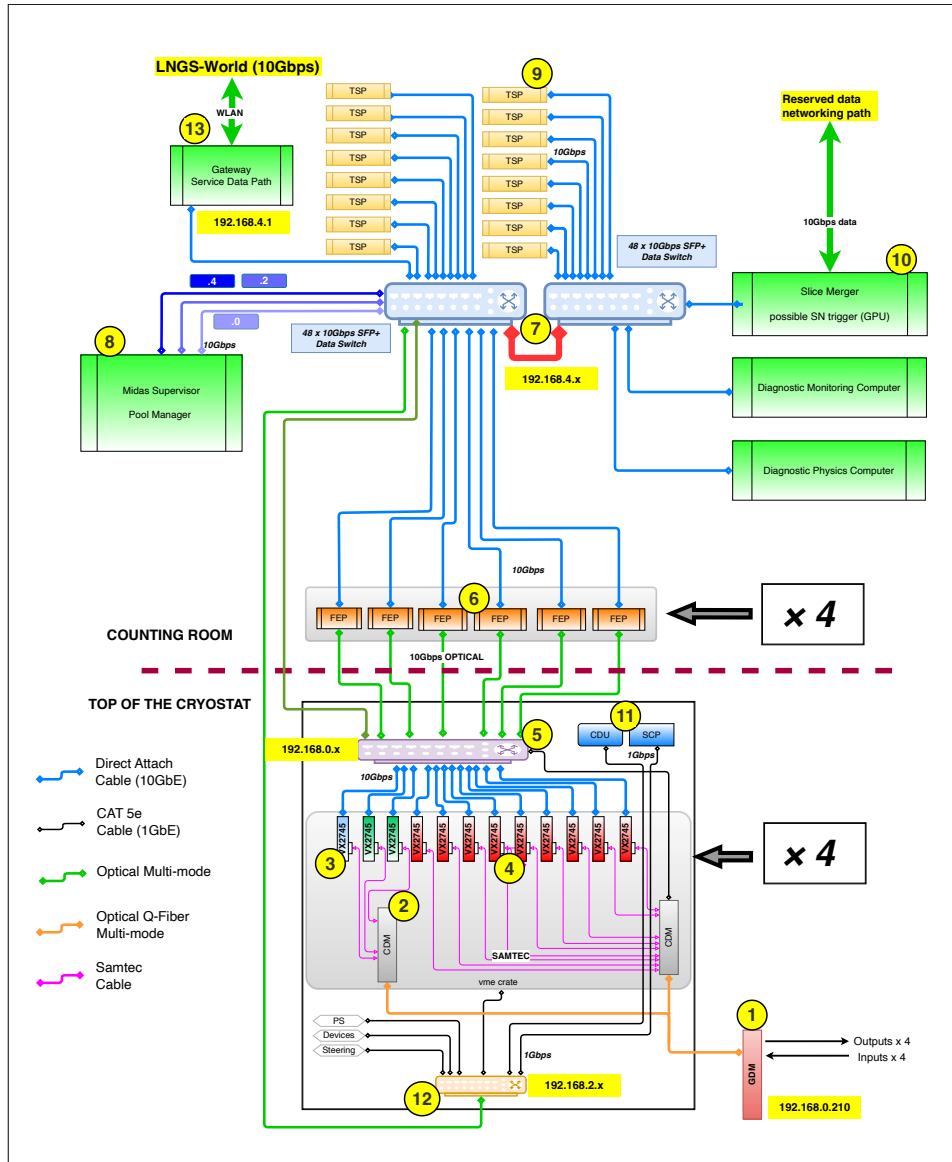


**Figure 2.** Schematic representation of the DAQ network. At the lower part of the diagram, the GDM (1) and the CDMs (2) are interconnected to distribute the clock and commands to the waveform digitisers (WFDs, for vetos and TPC, 3 and 4 respectively). Each digitiser is connected through a network switch (5) to dedicated FEP computers (6), where digitised waveforms are processed with a matched filter, and a peak finder is applied to identify *hits* within the waveform. Optical network cables connect the WFD network switches to the FEPs, which, in turn, are connected to a network data switch (7). These connections are implemented using individual optical links operating at 10 GbE. The Pool Manager (8) distributes the detector data to a cluster of TSPs (9), where online reconstruction is performed. Data from multiple TSPs are collected by the Merger machine (10) and stored on a local disk. The data traffic between the digitisers and the TSPs is managed by the DAQ server (8) acting as an interface to all DAQ components, integrating communication and hardware configuration (WFDs, GDM, CDMs) and DAQ SCP (11). This includes the management of CDUs (11), VME crates, and PDU power supplies through a network switch (12). Finally, the data are transferred for external storage through the Gateway machine (13) connected to the LNGS network.

The DAQ server (8) has the critical task of orchestrating the data traffic between the digitisers and the TSPs, the timing distribution and the acquisition sequences. This functionality is implemented by running Maximum Integrated Data Acquisition System (MIDAS), a publicly available, general-purpose software used in several small- and medium-scale physics experiments [10–12], through the MIDAS Supervisor. This DS-20k MIDAS server’s role is to interface to all the DAQ components, integrate communication, allow hardware configuration (WFDs, GDM, CDMs) and communicate with the DAQ SCPs (11). This includes the management of Cabinet Distribution Units (CDUs, 11), VME crates, and PDU power supplies (Power Supply (PS)) through a control switch (S2805S-24TF, 12).

Finally, the data are transferred for storage through the Gateway machine (13) connected to the external LNGS network.

## 2.1 DAQ infrastructure

The GDM and CDM boards, along with the digitisers and the network switch are located on top of the detector cryostat and grouped into 4 racks placed close to the chimneys equipped with signal feedthroughs. This location provides the shortest possible length of the signal cables to minimise noise pickup and signal integrity issues. Some elements of the Detector Control System (DCS) and specific safety interfaces will also reside in this area. All remaining machines are located in the DS-20k counting room, away from the detector.

The racks on the detector rooftop are standard closed 42U, 600×1000 racks. Their 1000 mm depth provides cabling space for the equipment. Dedicated fans will provide ventilation with ambient forced filtered air. The inner rack airflow temperature can be monitored with external temperature sensors available in the VME crate as well as at each of the WFDs (board and FPGA).

The DAQ racks hosting the main MIDAS servers, network switches, FEPs, TSPs, and DCS equipment will be placed in the IT room on the side of the detector infrastructure.

## 3 Time Slice Concept

The DAQ system of the DS-20k experiment is designed to operate in a fully triggerless mode, wherein each channel functions independently, continuously generating data without relying on a global trigger to initiate the acquisition. Instead, a local time-over-threshold logic at the single channel level is used to identify all waveform segments containing signal, without interrupting data acquisition.

Data selection for permanent storage occurs after signals from all detector components have been gathered into a single location and time sorted into data blocks called Time Slices (TSs). Figure 3 shows a pictorial representation of the TS timing. In this approach, the acquisition timeline is partitioned into intervals, each assigned later to a dedicated TSP for further analysis. Upon completing the processing of a TS, the TSP signals its readiness to handle the next one.

Due to the analysis time, a single TSP processes non-consecutive TSs. As a consequence, it cannot handle physics events that span between two neighbouring TSs. Such events require special handling. To address this issue, the end portion of each TS is duplicated and forwarded to the next TSP, ensuring boundary events are properly captured. The overlap corresponds to the maximum

electron drift time in the TPC, approximately 5 ms. Given a TS duration of 1 s, this overlap results in around 0.5% of the analysed events being duplicated at the DAQ output stage.

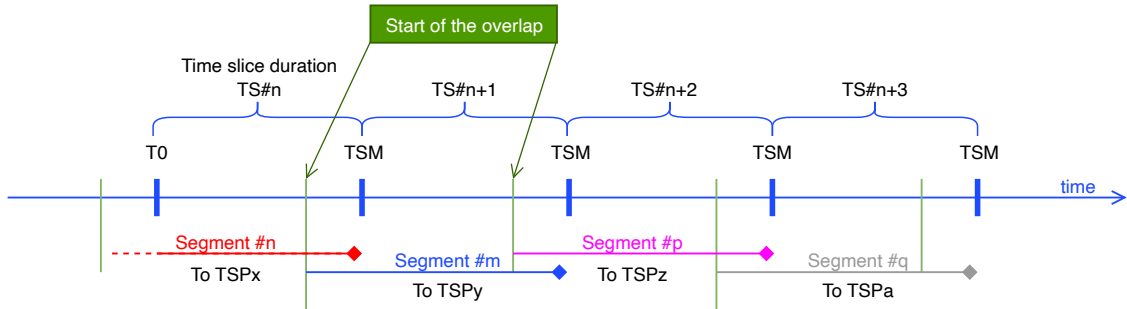


**Figure 3.** TS concept: the acquisition timeline is segmented into 1 s intervals, each directed to a dedicated TSP for further analysis. Since TSPs lack access to previously processed slices, a portion of each TS (5 ms) is duplicated and sent to the next TSP. Time Slice Markers (TSMs) ensure proper segment assembly (see section 5).

## 4 Waveform Digitisation and Filtering

Waveforms from the entire detector are transmitted as a differential signal to 48 commercial VX2745 CAEN 16 bit, 125 MS/s, high channel density (64 channels), 4 V peak-to-peak, 20 MHz bandwidth waveform digitizers [13] with 16 programmable analogue gains. The WFDs are placed in 4 crates, each containing 12 modules. Within a single crate, 9 out of 12 digitisers collect data from the TPC while the remaining 3 are used for the inner and outer veto.

The digitisers support the integration of custom firmware, which can be uploaded to a reserved section of the FPGA using the OpenFPGA service [14]. This feature grants direct access to the raw digital data stream, allowing for the implementation of custom acquisition control flows and data processing tasks such as triggering, data filtering and compression. Once these tasks are executed, control is returned to the CAEN firmware for data transmission via Ethernet to the FEPs.

The core FPGA in the VX2745 is a Xilinx ZU19EG [15]. This device has a Quad-coreARM<sup>®</sup> Cortex<sup>™</sup>-A53 MPCore<sup>™</sup> up to 1.5 GHz. The ARM System-on-chip manages the interface from the Programmable Logic to the Programmable System running Petalinux.

The digitiser data output format is 64-bit aligned, and the first five words are reserved for the header. The header includes multiple fields accessible to the user. The digitised waveform samples follow the header, each consisting of 16 bit samples stored sequentially.

The primary goal of the custom firmware is to implement a tailored trigger algorithm for identifying segments of the digitised waveforms containing at least one pulse corresponding to one or more photoelectrons. This process begins with the raw waveforms being processed through a 64-coefficient, 16-bit per coefficient Finite Impulse Response (FIR) filter, used to suppress high-frequency noise and maximise the signal-to-noise ratio. Each channel uses 16 Digital Signal Processors (DSPs) to construct the FIR filter.

Due to the limited available number of DSPs, and since some of them are needed for other functions, the input signal is processed at an effective sampling rate of 62.5 MS/s while the filter's DSPs run at 250 MHz, to reduce the filter's DSP usage. This configuration provides 4 filter clock cycles per input sample, enabling the application of 4 different coefficients per input sample over each sample interval. This allows the equivalent number of coefficients for each channel's filter to be 64, despite only 16 DSPs being used per filter. Each of the filter's output samples is then extended over 2 clocks, effectively reverting the original 125 MS/s signal rate.

Segments are retained if the signal exceeds the requirement for the duration of the amplitude above the threshold. Acquisition continues until the signal drops below a secondary, independently configurable threshold. A small post-trigger region is appended to each segment to extract key quantities, such as noise levels, while a short pre-trigger region captures baseline information. Finally, these complete signal segments are transferred to the FEPs [16].

This gated acquisition method maximises digitiser throughput while maintaining high peak detection efficiency. If a subsequent signal triggers the threshold during an ongoing acquisition, the gate is extended to include the additional signal and its post-trigger region. The gate extension is capped at a few tens of microseconds to avoid excessive data accumulation. Upon reaching this limit, the firmware truncates the waveform and resumes acquisition for subsequent segments once the signal falls again below the threshold.

Waveform segments exceeding the minimal duration threshold are divided into smaller sub-segments to accelerate data transfer due to time sorting in the factory-loaded firmware implementation. These sub-segments are reassembled at the FEPs stage (section 6).

All the parameters needed for the configuration of the boards can be modified by the user through the MIDAS webpage. A non-exhaustive list of the main configuration parameters and their function is provided in Table 1.

Each channel of the VX2745 features two First-In First-Out (FIFO) memory buffers: the PARAMS buffer and the WAVE buffer, the latter shown along with the subsequent stages of the data path inside the digitiser board in Figure 4. The PARAMS buffer stores metadata, including the channel number, timestamp, waveform size (in samples) and user-defined parameters. With a maximum depth of 512 64-bit words, it handles single-variable entries and is highly unlikely to overflow.

The WAVE buffer holds the waveform data with a maximum capacity of 4096 words (16384 samples). This buffer is susceptible to filling up during highly energetic or burst-like events, potentially creating a bottleneck for the system's data acquisition.

In addition to the per-channel PARAMS and WAVE, the VX2745 firmware implements a shared Sort & Merge buffer in the FPGA logic. This buffer collects data from all channels with a speed of 64 bit (4 samples) per 4 ns, (250 MHz). Since each 64-bit word contains four 16-bit samples, the corresponding effective throughput is 1000 MS/s, i.e. eight times the ADC (Analog-to-Digital Converter) sampling rate of 125 MS/s of the VX2745 modules. Measurements show, that in practice, due to limitations in the current firmware the achieved throughput is only a factor of five higher than the ADC readout rate, which may be lifted in future revisions. Waveform segments are then transferred to a 2 GB DDR4 memory with a speed of 64 bit per 5 ns (64 bit at 200 MHz).

A waveform segment is read as soon as its start time has been detected, and can only be transferred after its end time has been recorded. If a waveform remains above the trigger threshold,

Parameter	Type	Function
Readout channel mask	hex	Select active channels
Pre-trigger	int	Number of samples in the pre-trigger region
Post-trigger	int	Number of samples in the post-trigger region
Max segment length	int	Maximum length of a segment
Load pattern	bool	Load a collection of waveforms into the board
Enable decimation	hex	Enables waveform decimation
Decimation Factor	int	Decimation factor
Trigger threshold	int	Trigger threshold
Post-trigger threshold	int	Post-trigger threshold
Time over threshold	int	Number of samples over threshold
Enable FIR filter	hex	Enables onboard FIR filter
FIR coefficients	v[int]	64 coefficients for FIR filter
CDM veto enable	hex	Enables veto from CDM
WAVE FIFO almost full	int	Will go busy when there is this free space or less left.
PARAMS FIFO almost full	int	Will go busy when there is this free space or less left.
DC offset	v[int]	DC offset for the 64 channels

**Table 1.** Main configuration parameters for the CAEN VX2745 modules.

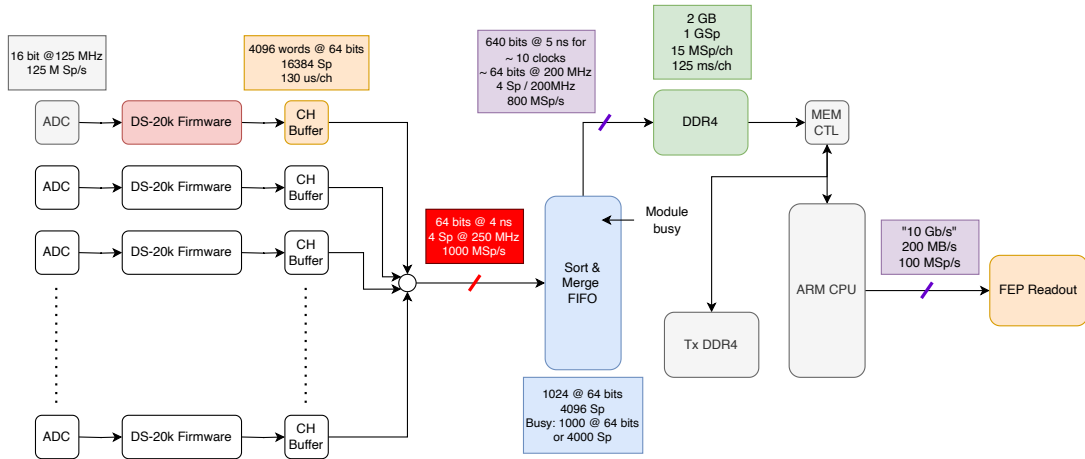


**Figure 4.** Schematic representation of the data path within the VX2745 boards. The Sort & Merge buffer collects data from all the channels (CH) with a speed of 64 bit at 4 ns, 250MHz. Since each 64-bit word contains four 16-bit ADC samples, this corresponds to an effective throughput of 1000 MS/s, i.e. eight times the ADC sampling rate of 125 MS/s. Waveform segments are then transferred to a 2 GB DDR4 memory with a speed of 640 b over about 10 clocks of 200 MHz then to an ARM CPU and finally to the FEPs.

subsequent segments with start times later than the ongoing waveform's start time are queued in a separate FIFO, regardless of their end times. For this reason, long waveform segments can delay the transfer of all earlier segments that have already fallen below the threshold but started after

the ongoing waveform. These delayed transfers can quickly fill the FIFO queue, posing a channel buffer overflow risk and requiring the management of the FIFO's own ALMOST FULL signal at the system level to avoid data loss. Figure 5 shows a schematic representation of the busy logic within a digitiser module. Black lines represent the data readout, while the red line represents the data transmission. Segment start and end times are identified by black and red arrows, respectively. A busy condition is asserted by the OR of individual channel ALMOST FULL signals. Upon asserting a busy, the signal travels to the corresponding CDM and back to the GDM, which suspends the acquisition for all the WFDs at the same time until the FIFOs are emptied. Finally, waveforms are transferred to the ARM CPU and the FEPs.

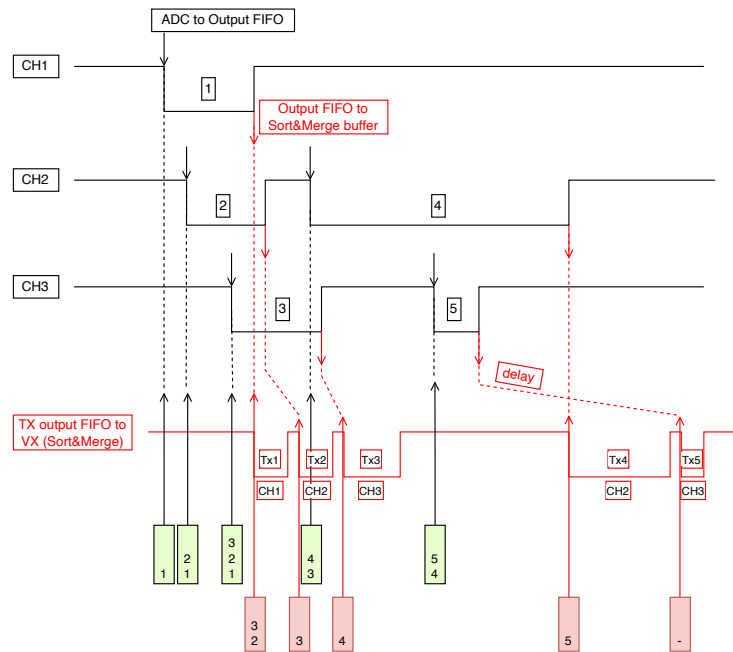


**Figure 5.** Schematic representation of the busy logic within a digitiser module. Black lines represent the data readout, while the orange line represents the data transmission. Segment start and end times are identified by black and red arrows, respectively.

There are several possible sources that could cause the digitiser board to assert a busy condition. At the module level, this might be caused by the backlog from the FEPs due to transmission or filtering. In this case, the readout is paused. If too large a portion of the DDR4 buffer is filled and the readout pause is long enough, then the Sort & Merge Buffer may assert a module busy.

At the individual channel level, long pulses on some channels preventing later channels from transferring their content to the Sort & Merge Buffer can cause an accumulation of pulses in the other channels' FIFOs with a subsequent overflow. This is considered the main source for asserting a module-level busy condition and has been studied with the help of a detailed simulation.

The software emulates a collection of 64 input waveforms generated by the DS-20k Monte Carlo (MC) background simulation and evaluates instantaneous WAVES buffer occupancy for each channel at a sampling period of 8 ns [17].

The simulation output was validated by cross-checking it against the same input fed to the digitiser using a special firmware version. This firmware implementation allows the loading of up to 1 ms of MC data in the digitiser at the nominal sampling rate 125 MS/s. Additionally, it provides analogue signals monitoring individual channel buffer occupancies, allowing for direct confirmation and validation of the software busy emulation.

The simulation shows that, in standard data-taking conditions, 4% of the waveforms in at least one of the digitisers reach 80% of the individual channel buffer. This behaviour can be mitigated by splitting the waveform segments into sub-segments to expedite data transmission, downsampling the waveforms within the digitiser and compressing the data in firmware. The splitting and downsampling algorithms have been implemented and tested. The implementation of compression is under development. A fast, two-stage, lossless compression algorithm has been implemented in VHDL and integrated into the Open FPGA firmware. The compression factor based on the DS-20k PDU waveform data has been measured to be better than 2. The algorithm combines first-order differential coding (delta coding) with Huffman entropy coding [18]. First, each sample is replaced by its residual with respect to the previous one. This reduces dynamic range as the most probable values are small, i.e. the probability concentrates near zero. In the second stage these residuals are encoded using Huffman code: each value in the range  $[-64, +64]$  is assigned a variable-length bit pattern according to its frequency in the typical waveform. Less frequent, out-of-range values start with the “escape” code followed by a raw 16-bit value. This means that a Lookup Table (LUT) must be first created based on a sample of expected waveforms. The LUT is indexed by the residual value. Each item contains two numbers: the length in bits of the encoded value and an upshifted bit template (padded with zeros to the required length in bits if needed).

At runtime, the encoder reads four data samples in two clock cycles, computes residuals, and accesses the LUT to retrieve codewords and their bit lengths. These are then concatenated and written to a small register buffer. When 64 bits (the equivalent of four samples of raw data) are accumulated in the buffer, they are transferred to the channel data FIFO. The buffer is then cleared and filled with overflow bits (if any). The coding operations are performed across four successive pipeline stages. The decompression algorithm is written in c++ and has been tested on the FEP machines. It can decode compressed data at the rate of 230 MB/s per core. The development of this algorithm allows the DAQ system to mitigate the potential busy issue, extend the maximal waveform segment length and increase the data rate from the digitiser to the FEP.

## **5 Global Data Manager and Crate Data Manager**

Because of the large channel number used in DS-20k multiple digitisers must work concurrently. A shared sampling clock is essential to ensure precise synchronisation in phase and time across all digitisers. Precise absolute time, while not relevant for a Dark Matter search with DS-20k, is required for correlation of supernova burst events, with signals detected by other detectors worldwide, while phase synchronisation of all channels is necessary for proper event reconstruction.

A synchronisation signal packet is delivered by the LNGS to the underground laboratory via optical fibre to allow for assigning accurate timestamps to events by all experiments [19]. This packet is constructed at the surface facility and is based on a GPS signal. The packets are sent

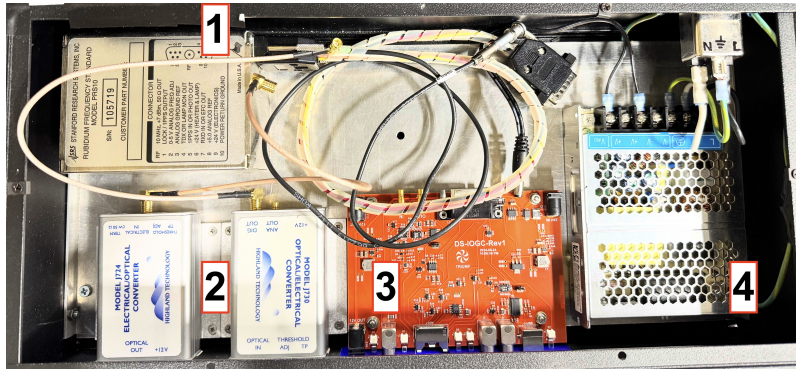


**Figure 6.** The picture shows a crate box with Stanford Research System PRS10 rubidium clock (1), optical/electrical and electrical/optical converters (2), a custom input-output GPS Clock board (IOGC, 3) developed in TRIUMF and a power supply (4). The synchronisation signal is delivered by the LNGS laboratory by optical fibre; the signal is converted to electrical and delivered to the rubidium clock through the IOGC board, which in turn is connected through the samtec connector to the GDM. The electrical/optical converter will be used for calibration by sending a signal through LNGS infrastructure, allowing for precise measurement of the synchronisation signal delay.

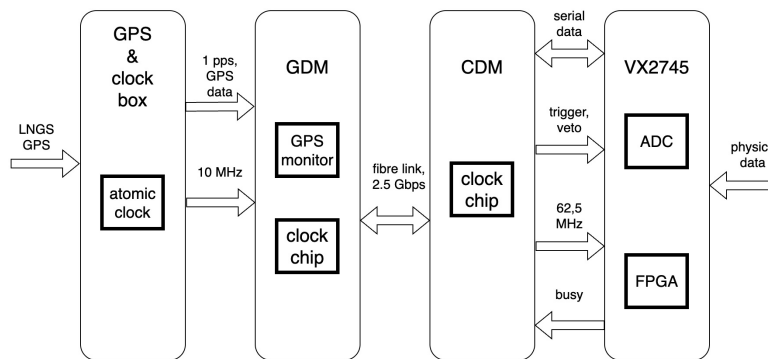


**Figure 7.** Schematic representation of the clock distribution and data management with the GDM and CDM boards. From the left: the timing information is delivered to the underground laboratories by LNGS with the optical fibre signal formed in the surface laboratory based on the GPS data. This signal is used to drive the local Rb clock. The LNGS stream is converted to electrical and, in parallel with 10 MHz signal from the atomic clock, transferred to the GDM located nearby the clock box. The GDM decodes the absolute time correcting for the signal delay from the surface laboratory. The optical links operating at 2.5 Gbps are used to distribute the phase-aligned recovered clocks and time-synchronous control packets to 8 CDM boards which in turn send it to all the 48 digitizers.

at 1 Hz rate and the first edge marks the synchronization time. Each data packet comprises the absolute time of the previous packet and the GPS clock bias correction expressed in nanoseconds. This signal is fed to a custom input-output GPS Clock board (IOGC, see Figure 6) and disciplines a local atomic clock (Stanford Research System PRS10 rubidium frequency standard [20]). The system is able to provide absolute time with an accuracy of 15 ns. In case of loss of the LNGS synchronisation signal, the PRS10 clock can hold a Stratum 1 level for 72 hours.

Figure 7 displays a schematic representation of clock distribution and data management in DS-20k. Two custom data manager boards were developed at TRIUMF for DS-20k: the GDM and CDMs (1 and 2 in Figure 2 respectively). The reference 10 MHz clock maintained by PRS10 atomic clock together with 1 Hz LNGS synchronization signal are delivered to the GDM board. The single GDM board is connected to 8 CDMs. In each crate, 1 CDM controls digitisers collecting data from the TPC (9 out of 12), and the second one controls the remaining digitisers 3 used for the inner and outer veto.

This design results in the DAQ infrastructure having a unique clock distributed from the GDM to the digitisers through multiple CDMs located near the different groups of digitisers. The communication between the GDM and the CDMs occurs via an optical link operating at 2.5 Gbps. Optical links are configured in real time to distribute phase-aligned recovered clocks and time-synchronous control packets to all digitisers. The synchronisation between the digitisers is achieved by distributing a single, highly stable, phase-aligned clock signal to all data converters. The phase shift of the data between the channels within a single WFD and between WFDs has been measured by feeding an identical sine wave signal through a waveform generator connected to a fan-out. The maximum time shift is measured to be below 500 ps for any channel and digitiser pair.

The synchronised time segmentation mechanism requires transmitting a Time Slice Marker (TSM) to all the digitisers to ensure proper segment assembly. The data packets transmitted from the CDMs to the digitisers are decoded and reformatted for communication at a frequency of 125 MHz, which is dictated by the limitations of the digitiser hardware components. A phase-aligned 62.5 MHz clock, derived from the 125 MHz source, is routed to the front panel of the digitisers, serving as the main clock.

Full-duplex communication is used to transmit various data packets: reference clock, TSM, operation control, external trigger and reception of real-time hit map from all the channels. Each control packet contains critical components: the TSM is utilised during the merging of data fragments in the FEPs, specifications regarding the trigger type and sector address are essential in case of triggered operation of the DAQ system, a single bit in the control packet is used as a veto to suspend and resume data acquisition to prevent data loss. For this purpose, each WFD provides a busy signal that is asserted when its buffer occupancy reaches a predefined threshold (section 4). This mechanism allows the system to react promptly, suspending acquisition across all digitisers to ensure complete and accurate TS data collection, which is essential for proper event reconstruction.

The TSM bit, along with locally stored and time-corrected LNGS time information, triggers a TSM event in the WFD. Each digitiser generates a single TSM event marked with a bit in the header and the time information encoded in the data section. The TSM event is transferred to the FEP and does not contain any waveform data. This event is essential for merging data fragments across all the digitisers and detecting any missing fragments within the FEPs.

Furthermore, the control packet includes command fields for external trigger requests originating from the GDM, which can initiate the acquisition of the currently buffered data in the digitisers. These external triggers may stem from inputs available on the GDM, such as test pulses, calibration devices or algorithmic decisions based on the hit-map received from the digitisers. This comprehensive control mechanism ensures precise data acquisition and effective synchronisation across the system.

## 6 Front End Processors

The FEPs are responsible for several tasks. They acquire waveform data from the CAEN VX2745 digitisers and perform single-channel data processing, which includes single waveform segment digital filtering and data reduction. Additionally, the FEPs time sort the event data across all the connected VX2745 units (each FEP reads data from 2 digitisers) in time slices based on the TSM counter and listens for commands from the Pool Manager (PM) application to initiate the transfer of the TS data to the next idle TSP.

These tasks run concurrently in separate threads to optimise CPU usage and network bandwidth. The communication between threads is based on software queues. One thread per board is responsible for reading the data. Another thread processes the queue, subtracts baselines and applies filtering to all waveforms. Finally, an additional thread is responsible for building and shipping the TS.

The primary physics function of the FEPs is waveform data processing, which involves extracting the time and prominence of all peaks within the segments received from the digitisers, where each peak corresponds to one or more photoelectrons. The waveform data processing algorithm operates in steps to efficiently identify these peaks. The first one involves removing the baseline from the raw waveform segment. The baseline values are calculated as the average of a predetermined fixed number of samples in the first part of each waveform segment. Next, each waveform receives a calibration to equalise the gains across all the detector readout channels. Then, the baseline-subtracted and calibrated waveform is processed using an infinite response Auto-Recursive exponential filter.

The hit finding algorithm was developed to improve real-time hit identification and is based on the difference between the matched exponential filter and a moving average filter. The matched filter maximises the signal-to-noise ratio and produces sharp, cusp-like peaks at the hit positions. Subtracting a moving average of the filtered waveform suppresses slow baseline variations and correlated low-frequency noise, allowing individual hits to be clearly separated. Three key parameters govern the hit-finding algorithm: the moving average's window length, the hit detection threshold level, and the charge-to-prominence cut-off. Hits must cross a specified threshold and exhibit a charge-to-prominence ratio greater than a predetermined minimum value to be retained. A preliminary optimisation of the algorithm on simulated data indicates that 99% efficiency on single photo-electron signals can be reached with  $O(10 \text{ Hz})$  of noise-induced fake signals. The FEPs calculate the prominence, charge and time position of each hit. These, together with information on the individual waveforms (time, duration, integrated charge and number of identified hits) constitute the only information transmitted in standard data taking conditions to the subsequent DAQ stages while the individual waveforms are discarded.

Figure 8 shows the waveform processing performed by the FEPs from the filtering to the hit finding stage.

Additionally, all the waveform segments over the full TS duration coming from the 128 channels (64 per module) are decimated and separately summed for the top and bottom channels with reference to the beginning of the time slice and encoded in Zero Length Encoding (ZLE) format [21–23] to be transferred to the TSPs, together with the information on hits and the summary information about individual waveform segments discussed above. This format enables a zero suppression of

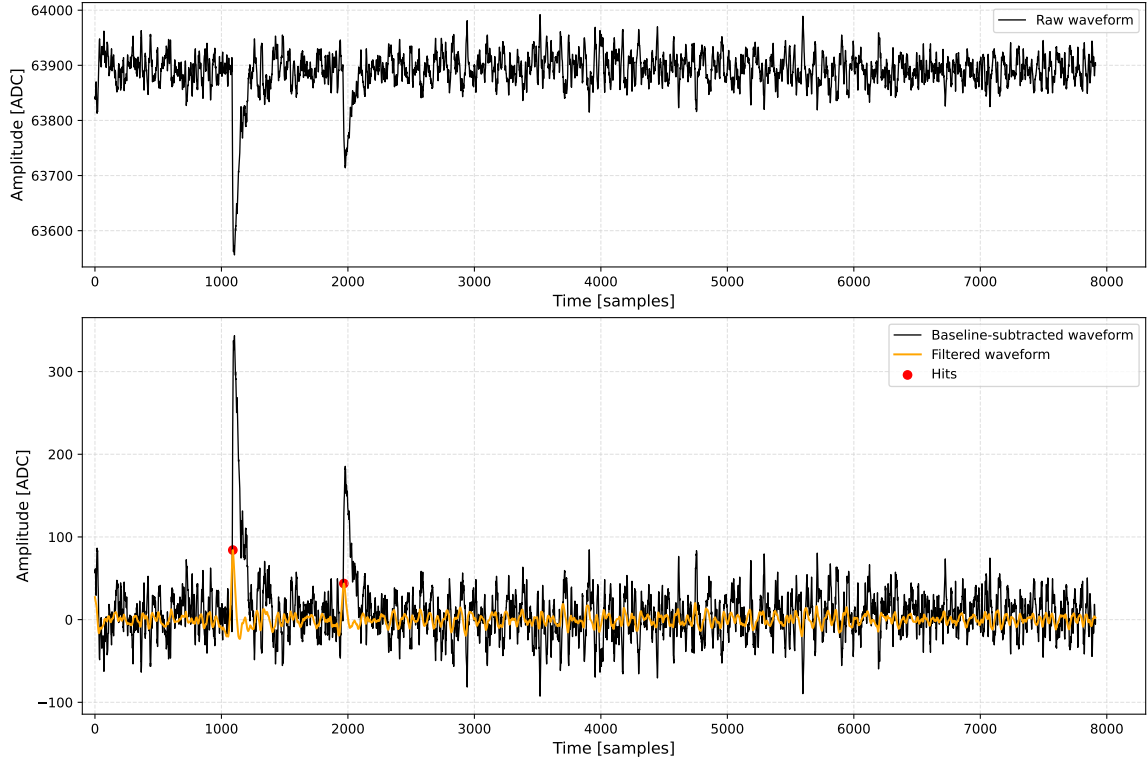


**Figure 8.** Waveform processing in the FEP. Baseline-subtracted waveforms are first filtered using an Auto-Recursive exponential filter (yellow line), and then a peak finder is applied (red points). The peak finder looks for signals exceeding a preselected threshold in the moving average-subtracted waveform. Only signals exhibiting a charge-to-prominence ratio greater than a predetermined minimum value are retained.

the regions where no signal has been detected, thus reducing the data throughput. In this respect, a further cut on the summed waveform amplitude might be applied at this stage.

Finally, the FEPs are responsible for monitoring the channels and assessing the raw data quality. A waveform and a reduced data stream are periodically extracted at the FEP level and transmitted to a remote analysis processor via the MIDAS event transfer system. This channel monitoring ensures data integrity while minimising the potential impact on extracting physics information. Various relevant metrics, such as prominence histograms, raw segment charges and baselines, are continuously assessed and displayed on a dedicated MIDAS webpage during this monitoring process.

## 7 Data Flow Control, Pool Manager (PM) and Midas supervisor

Data transfer from FEPs to TSPs is orchestrated by the PM application, which runs on the MIDAS server. The primary role of the PM is to assign the appropriate TSP address to each FEP for a given TS transmission. A pictorial representation of the DS-20k data flow is displayed in Figure 9.

The PM maintains an idle processor queue implemented as a FIFO data structure, which stores identifiers of the TSPs (TSP-ID) ready to process a new Time Slice. The PM continuously scans this

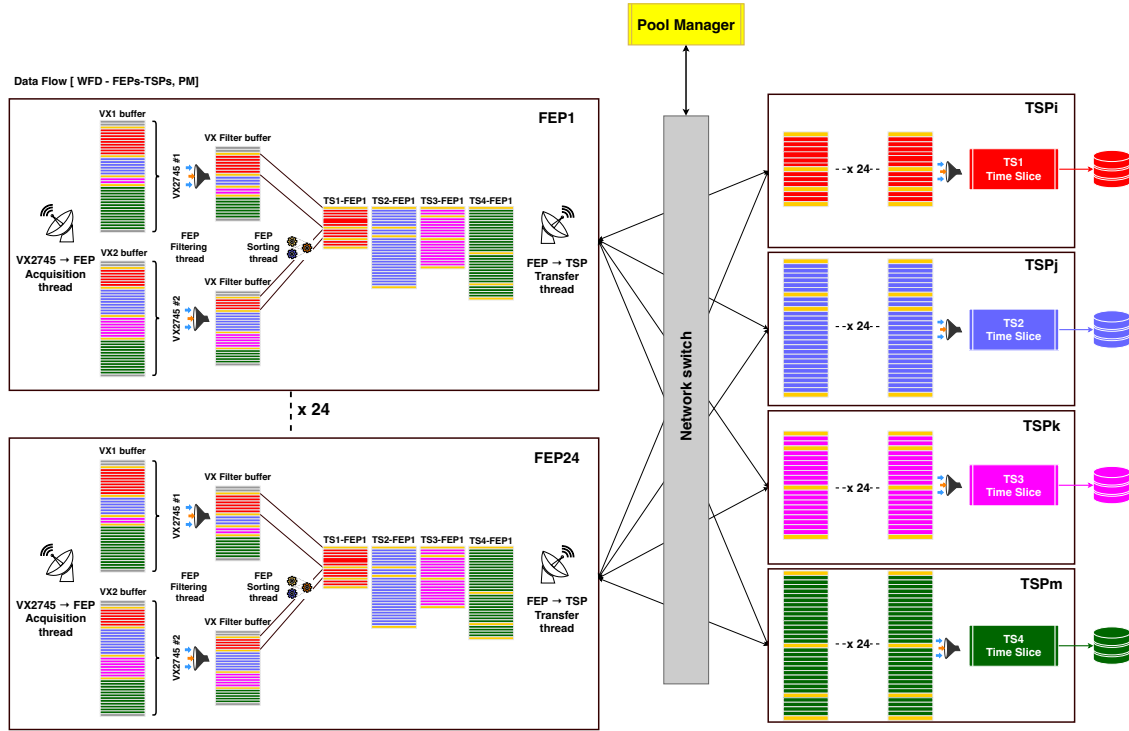


**Figure 9.** Schematic representation of the data flow in DS-20k. Data are transferred from the waveform digitisers (WFDs) to the FrontEnd Processors (FEPs), where they are sorted in time and organised in 1 s Time Slices (TSs). In the picture, fragments having the same colour belong to the same TS. TSs are then sent from the FEPs to the TSP through the network switch, under the Pool Manager’s (PM) supervision. The PM assigns the appropriate TSP address to each FEP, enabling the transmission of TS data.

queue, retrieves the oldest TSP-ID, and pairs it with the next available Time Slice-ID, forwarding this information to all the FEPs. Each FEP then stores the TSP-ID and corresponding Time Slice-ID in its queue, allowing multiple TS data segments to be simultaneously transferred to available TSP destinations. This parallel processing scheme significantly optimises network bandwidth utilisation.

Once data have been transferred to the TSPs, the PM, while waiting for the reception of the summary notification packets from any active TSP, will direct the next TS data packet to the next idle TSP.

Once a TSP has completed the analysis of its assigned TS, it is responsible for notifying the PM. This communication includes a notification of the analysis completion status and a detailed report on the outcome of the most recent TSM analysis.

The notification message is composed of a TSP-ID (TSP node ID), the TS-ID, representing the number or identifier of the completed TS, the transfer time, indicating the duration required to transfer the TS from the FEPs to the TSP, the size of the TS, the time taken to analyse the slice, and the output data size, generated after the completion of the analysis.

Upon receiving the notification packet, the PM processes it in two steps. First, the PM adds the TSP-ID to the idle processor queue, making the TSP available for handling the next TS. Second, the

PM composes an event status for the recently completed TS. This status and related information are integrated into the MIDAS software infrastructure. They can be accessed via a custom web history page, allowing real-time monitoring and review of processing events.

Communication between the TSP, PM, and FEPs occurs through the central data switch using ZeroMQ (ZMQ) asynchronous messaging library, which provides an efficient method for message broadcasting [24]. Despite sharing the main data network, the communication overhead introduced by ZMQ is minimal and has a negligible impact on overall data transfer performance.

The MIDAS software package manages the overall data acquisition system. It performs several key functions: configuring the readout equipment, orchestrating the run sequence, generating various alarm levels (e.g., warnings, errors, or custom alarms) based on user-defined criteria, controlling data transfer to analysis tools, recording data for permanent storage, and managing equipment operation and monitoring. Additionally, MIDAS provides an application framework for device interfaces.

In the DS-20k experiment architecture, while MIDAS continues to handle overall control and monitoring, its role has been specifically adapted to manage data flow control only, rather than data transfer. This architectural decision enables raw socket data transfer from the Digitizers to the TSPs, allowing for optimal data throughput in the system.

## **8 Time Slice Processors and Merger**

TSPs manage incoming connections from the FEPs, receiving their data payloads. Once a TS is processed, the TSP notifies the PM and waits for the next TS.

The primary role of TSPs is to collect and select hits to ensure efficient data processing. Additionally, they complete the sum of all the top and bottom channels by adding up the partially summed waveforms received from the FEPs.

The TSPs' functionality can be extended to perform more advanced analyses, including event classification, and anomaly detection.

Events can be categorized into different types, such as: Regular DM (e.g. S1 in the WIMP region of interest), high energy gammas in the TPC for calibration (e.g. high energy S1), low energy S2 events (e.g. low multiplicity S2 pulses isolated from other pulses), and Inner/Outer Veto (e.g., pulse above the threshold necessary for cosmogenic suppression and calibration or monitoring). This classification process allows the system to pre-scale specific event types, thereby reducing data storage requirements, if needed. By performing these analyses, the TSP generates a new set of data that is stored locally on each TSP's storage device.

Time slices showing statistically significant anomalies, like an excess of low energy signals characteristic of a neutrino burst from a core-collapse supernova within the galaxy [25], can be tagged for further quasi-online analysis downstream.

Each TSP maintains its file composed of non-consecutive TSs for the run period, while the PM records the TSs IDs processed by each TSP. TSPs notify the PM at key stages of their operations: when the analysis of a TS begins, if the analysis fails, and when the transmission of the TS to the following data acquisition stage is completed. The PM then forwards this information to the Merger, the machine responsible for collecting the TSs.

The Merger receives the TSs from the TSPs via raw TCP/IP sockets, sorts the TSs chronologically and concatenates them into a continuous data stream. Once sorted, the TSs are stored locally for temporary storage. In case of transmission failure between a TSP and the Merger, the local TSP copy is to be used to retrieve the TS. In addition, it handles the transfer of the concatenated TSs to the Centro Nazionale Analisi Fotogrammi (CNAF) data centre for long-term storage and offline analysis. A 100 TB local disk, corresponding to approximately one week of data taking, will be kept and deleted once the transfer has been acknowledged.

The Merger continuously monitors for missing TSs during data collection. If a missing TS is detected, it checks the PM logs to determine the status of the corresponding TSP. If the analysis has failed, the slice is marked as irrecoverable and no longer considered missing. However, if the analysis has started but not yet completed, the Merger waits for a predefined time before proceeding to the next TS.

TSs not immediately delivered to the Merger remain temporarily stored on the corresponding TSP until successful transmission, ensuring robustness against acquisition delays or failures without data loss.

Beyond sorting and concatenating TSs, the Merger also delivers anomaly-tagged slices together with a predetermined number of preceding and following TSs to a dedicated processor, possibly equipped with GPUs, implementing, e.g. a fast supernova trigger. It will analyse, in quasi real-time, the collected TSs for anomalous event rates across the TPC and Veto volumes. If a potential supernova event is detected, this processor can trigger an alert. This alert might then be sent to SNEWS 2.0.

## 9 Slow Control

The DS-20k Slow Control (SC) system comprises two complementary components: the DAQ SC and the DCS, as shown in Figure 10.

The SC manages devices integral to the data acquisition process, including SiPM readout electronics, power supplies, and steering control. It is also used to oversee the DAQ racks together with all its components. The SC ensures real-time monitoring and regulation of the power and temperature of the digitizers, CDMs, HV and HV power supplies, CDUs and network switches. The SC is operated by a dedicated computer and provides the network interface to the DCS.

The DCS independently controls and monitors the critical detector infrastructure, including the cryogenic system (both AAr and UAr) and the TPC high-voltage system for drift and electroluminescence fields.

Commercial HV units provide the precision current monitoring required for individual channel I–V curve measurements, together with a “steering” system for channel and PDU activation. The latter is composed of a *warm* module interfacing with the DAQ and a *cold* electronics circuit on the PDU motherboard. The control through the steering system has several functions: turning on and off individual channels, turning on and off the LV and HV of the 16 Tiles independently and turning on and off a microcontroller needed to send a PDU unique identifier to the DAQ. A unique bias voltage per PDU, hence four analogue channels, is present.

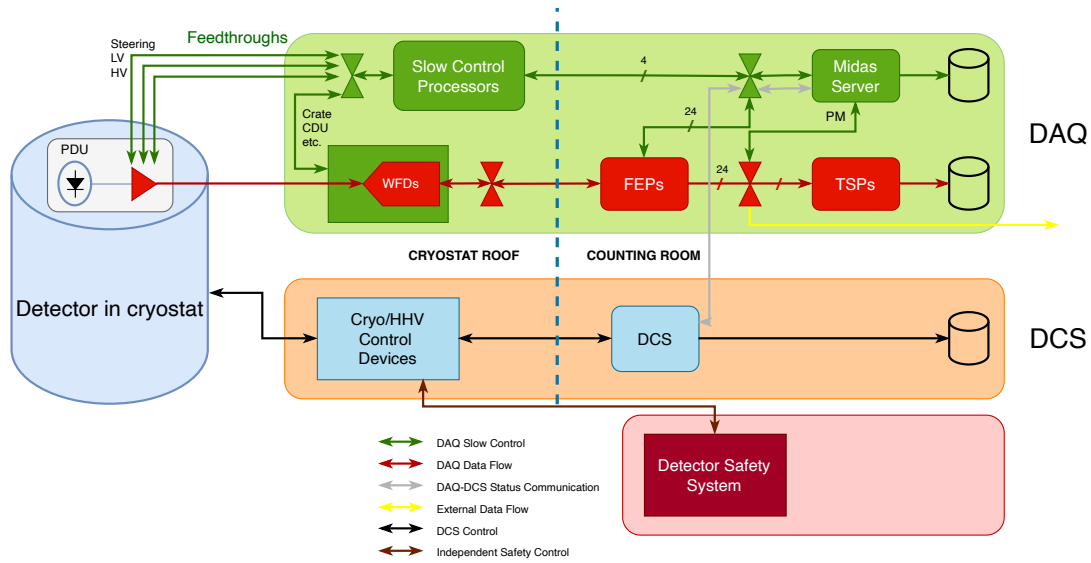


**Figure 10.** DS-20k Slow Control (SC) system, structured in two complementary components: the DAQ SC and the DCS. The SC manages devices integral to the data acquisition process, including SiPM readout electronics, LV and HV supplies, steering control, and VME crates. The DCS independently controls and monitors critical detector infrastructure, including the cryogenic system (both AAr and UAr) and TPC high-voltage system for drift and electroluminescence fields. The blue dashed line separate the equipment that will be positioned on top of the cryostat and in the experiment counting room.

Using the CERN WinCC-OA Supervisory Control and Data Acquisition (SCADA) framework ensures stable, real-time monitoring and data exchange to and from the DAQ for detector and status validation [26]. Information exchange and direct device access enhance redundancy and reliability.

A Detector Safety System (DSS) based on a dedicated Programmable Logic Controller (PLC) safeguards equipment and personnel by interfacing with the cryogenic and TPC subsystems. It connects directly to TPC hardware and PDU power supplies through interlocks managed over an Uninterruptible Power Supply (UPS)-backed network, with additional interlocks securing the cryogenic system.

## 10 Quadrant Test

"Quadrant", i.e. 1/4 of the DS-20k DAQ system, has been realized in TRIUMF Laboratory, Canada, for development and testing (see Figure 11). It was composed of one GDM and one CDM board, 12 VX2745 boards, one 10 GbE network switch, 6 FEPs, optical link connection to 5 TSPs, external clock interface and an analogue fan-out connected to the waveform generator for synchronisation tests. A 64 GB memory SuperMicro AS-2015A-TR machine has been chosen to host the MIDAS supervisor.

The Quadrant setup has been stress-tested by using a 2 kHz periodic trigger simultaneously on all the 768 channels from the 12 digitisers. This configuration corresponds to the worst-case

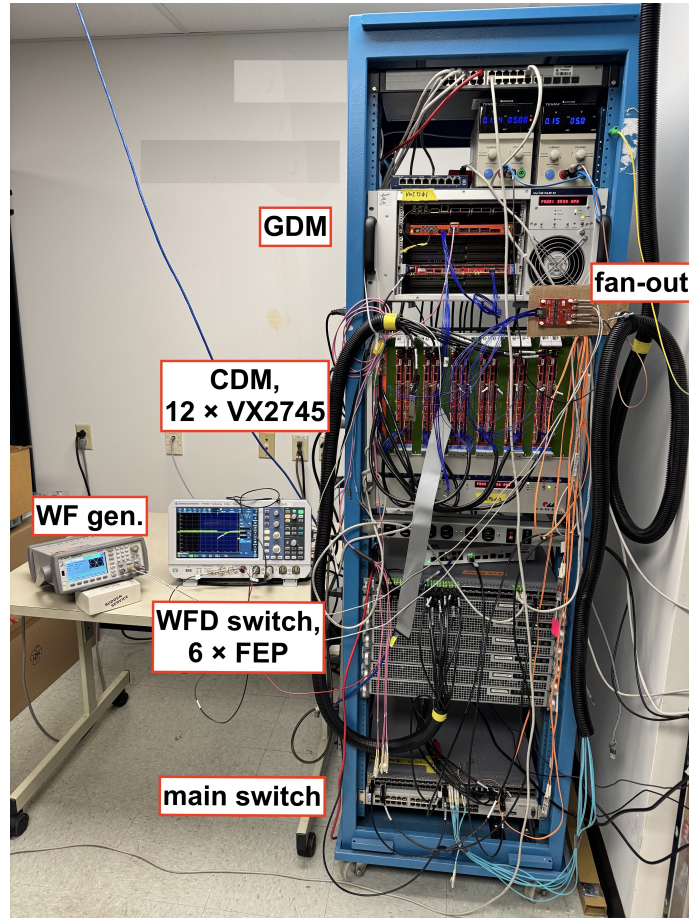


**Figure 11.** The picture shows the Quadrant setup built and tested in TRIUMF, Canada. It corresponds to one of the final system's four identical racks, including 12 waveform digitisers (WFDs) and 6 FEPs. Not shown are the TSPs located in a separate rack and the MIDAS Supervisor.

scenario when all the channels are triggering at the same time. The length of the acquired waveforms was set to  $8 \mu\text{s}$ . A sustainable data rate of 250 MB/s has been measured on each digitizer board without any lagging and is limited by the FEP data handling performance, while the connection between the digitizer board and the FEP allows for higher data rate transfer of 10 GbE ensuring a safety margin. The measured rate is presented in Figure 12. The FEP processor usage is below 60% for any thread. The data rate from the FEP to the TSP during this test was 8 MB/s. The system demonstrated stable operation over long operation (300 h). Finally, the full TS architecture has been implemented and tested with part of the Quadrant setup.

## 11 Conclusions

One of the challenges of DS-20k experiment is the development of a robust DAQ system enabling continuous signal acquisition from its 2720 channels. The successful implementation of the DAQ system architecture presented here demonstrates that such a system can be built largely from commercial components allowing for easy scalability. The CAEN VX2745 digitizers provide high

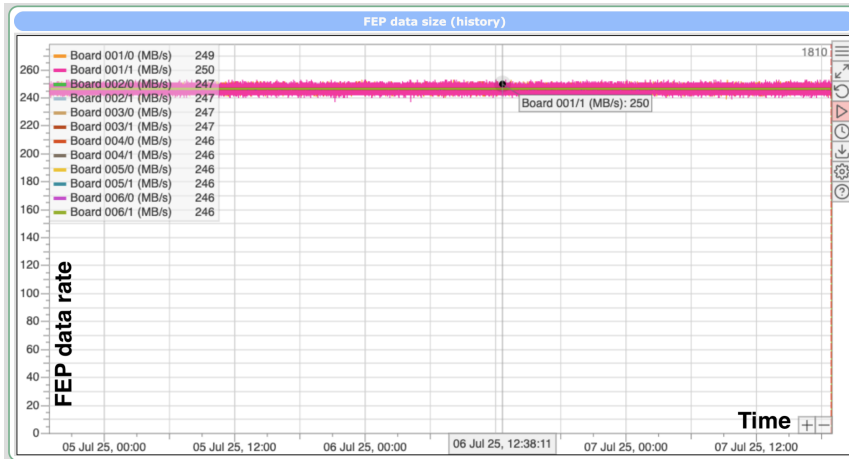


**Figure 12.** Plot presents the data rate in MB/s from 12 digitizer boards to the FEP machines over a period of 2.5 days. The rate was stable for all boards at 250 MB/s.

channel density and flexibility thanks to the programmable OpenFPGA. Multi-board synchronisation of 48 modules with custom Data Manager boards ensuring sub-nanosecond synchronisation across all digitisers through a rubidium standard disciplined by LNGS signal, enabling coherent sampling and accurate time segmentation for event reconstruction and absolute time information essential for the supernova events.

The distributed processing based on Front End Processors and a scalable farm of Time Slice Processors allows for online hit extraction, data reduction, event classification, and possible extension of additional algorithms without impacting the data flow.

The successful commissioning of the Quadrant system in TRIUMF representing one quarter of the final DAQ confirms the feasibility of the full design. Sustained operation at 250 MB/s per digitiser with simultaneous trigger demonstrates that the system satisfies the throughput and stability required for physics data taking. The data synchronisation test showed coherent timing of the data acquisition with an intra-channel spread well below the sampling period.

## Acknowledgments

We would like to thank the other scientists and technical staff for their essential contributions throughout the course of this work, in particular Ian Johnson (jTechnologies) for the development of the digitizer firmware, Peter Margetak (TRIUMF) for the design and production of custom boards, and Samuel de Jong (University of Victoria) for his contributions to the FPGA firmware. We also acknowledge the support and assistance provided by the staff at CAEN.

This work was supported by the U.S. National Science Foundation (NSF) through Grants No. PHY-0919363, PHY-1004054, PHY-1004072, PHY-1242585, PHY-1314483, PHY-1314507, PHY-1622337, PHY-1812482, PHY-1812547, PHY-2310091, PHY-2310046, associated collaborative grants No. PHY-1211308, PHY-1314501, PHY-1455351 and PHY-1606912, as well as Major Research Instrumentation Grant No. MRI-1429544. Additional support was provided by the

Pacific Northwest National Laboratory, operated by Battelle for the U.S. Department of Energy under Contract No. DE-AC05-76RL01830.

Support was provided by the Istituto Nazionale di Fisica Nucleare (INFN), through grants from the Italian Ministero dell’Istruzione, Università e Ricerca, including Progetto Premiale 2013 and Commissione Scientifica Nazionale II, as well as by the PRIN2020 project of the Italian Ministry of Research (MUR) (Grant No. PRIN 20208XN9TZ).

This work was supported by the Natural Sciences and Engineering Research Council of Canada, SNOLAB, and the Arthur B. McDonald Canadian Astroparticle Physics Research Institute. Support was received from the French government from LabEx UnivEarthS (ANR-10-LABX-0023 and ANR-18-IDEX-0001). Additional support was received from the IN2P3-COPIN consortium (Grant No. 20-152).

This work was supported by the Chinese Academy of Sciences (113111KYBS20210030) and the National Natural Science Foundation of China (12020101004). Support was provided by the São Paulo Research Foundation (FAPESP) under Grant No. 2021/11489-7 and by the National Council for Scientific and Technological Development (CNPq). Support is acknowledged from the Deutsche Forschungsgemeinschaft (DFG, German Research Foundation) under Germany’s Excellence Strategy — EXC 2121: Quantum Universe — 390833306.

The authors acknowledge support from the Spanish Ministry of Science and Innovation (MICINN) through Grants PID2022-138357NB-C22 and PID2022-138357NB-C21 and the Atracción de Talento Grant 2018-T2/ TIC-10494.

This work was supported by the Polish National Science Centre (NCN) through Grants No. UMO-2022/47/B/ST2/02015 and UMO-2023/51/B/ ST2/02099, by the Polish Ministry of Science and Higher Education (MNiSW, Grant No. 6811/IA/SP/2018). This work was supported by the FNP IRA programmes: AstroCeNT (MAB/2018/7), funded from the ERDF, and Astrocent (FENG.02.01-IP.05-A015/25) co-financed by the European Union under FENG 2021–2027; and Teaming for Excellence grant Astrocent Plus (101137080) funded by the European Union with complementary national funding from the MNiSW (MNiSW/2025/DIR/811).

This project received funding from the European Union’s Horizon 2020 research and innovation programme under Grant Agreement No. 952480 (DarkWave).

Support was provided by the Science and Technology Facilities Council, part of United Kingdom Research and Innovation, and by The Royal Society.

## References

- [1] The Global Argon Dark Matter Collaboration, *Darkside-20k technical design report*, Tech. Rep. DARKSIDE-CSN2-TDR-2112– v3.0 Submitted to INFN, The Global Argon Dark Matter Collaboration, INFN, Assergi, Italy (2021).
- [2] F. Acerbi et al., *DarkSide-20k sensitivity to light dark matter particles*, *Communications Physics* **7** (2024) .
- [3] A. Razeto et al., *Very large SiPM arrays with aggregated output*, *Journal of Instrumentation* **17** (2022) P05038.
- [4] F. Acerbi et al., *Quality Assurance and Quality Control of the 26 m<sup>2</sup> SiPM production for the DarkSide-20k dark matter experiment*, 2024.

- [5] P. Agnes and et al., *First results from the darkside-50 dark matter experiment at laboratori nazionali del gran sasso*, *Phys. Lett. B* **743** (2015) 456.
- [6] C. Benson, G.D. Orebi Gann and V. Gehman, *Measurements of the intrinsic quantum efficiency and absorption length of tetraphenyl butadiene thin films in the vacuum ultraviolet regime*, *The European Physical Journal C* **78** (2018) .
- [7] D. Montanari et al., *Development of membrane cryostats for large liquid argon neutrino detectors*, *IOP Conf. Ser. Mater. Sci. Eng.* **101** (2015) 012049.
- [8] R. Kugathasan, *A low-power mixed-signal ASIC for readout of SiPM at cryogenic temperature*, *PoS TWEPP2019* (2020) 011.
- [9] S.A.K. et al., *SNEWS 2.0: a next-generation supernova early warning system for multi-messenger astronomy*, *New Journal of Physics* **23** (2021) 031201.
- [10] S. Ritt and P. Amaudruz, *New components of the MIDAS data acquisition system*, in *1999 IEEE Conference on Real-Time Computer Applications in Nuclear Particle and Plasma Physics. 11th IEEE NPSS Real Time Conference. Conference Record (Cat. No.99EX295)*, pp. 116–118, 1999, DOI.
- [11] M. Köppel, *Data Flow in the Mu3e DAQ*, *IEEE Transactions on Nuclear Science* **70** (2023) 898.
- [12] M. Thorpe, C. Angelsen, G. Barr, C. Metelko, T. Nicholls, G. Pearce et al., *The T2K near detector data acquisition systems*, in *2010 17th IEEE-NPSS Real Time Conference*, pp. 1–8, 2010, DOI.
- [13] “CAEN VX2745 64 Channel 16 bit 125 ms/s Digitizer with Programmable Input Gain.” <https://www.caen.it/products/vx2745/>.
- [14] “OpenFPGA.” <https://www.caen.it/families/open-fpga-digitizers/>.
- [15] “Xilinx ZU19EG.” <https://xilinx.com/products/boards-and-kits/1-14u9g6z.html>.
- [16] “DPP-ZLEplus.” <https://www.caen.it/products/dpp-zleplus/>.
- [17] P. Agnes et al., *Simulation of argon response and light detection in the darkside-50 dual phase tpc*, *Journal of Instrumentation* **12** (2017) P10015–P10015.
- [18] D.A. Huffman, *A method for the construction of minimum-redundancy codes*, *Proceedings of the IRE* **40** (1952) 1098.
- [19] M.D. Deo, G.D. Carlo, W. Fulgione, A. Molinaro, S. Parlati, R. Podviianiuk et al., *Accurate gps-based timestamp facility for gran sasso national laboratory*, *Journal of Instrumentation* **14** (2019) P04001–P04001.
- [20] “PRS10 — Low phase noise Rb oscillator.” <https://www.thinksrs.com/products/prs10.html>.
- [21] “Zero Length Encoding firmware.” <https://www.caen.it/caen-digitizer-whitepaper/>.
- [22] K.I. Duwe, “Data Reduction Techniques.” [https://hps.vi4io.org/\\_media/teaching/wintersemester\\_2015\\_2016/pre-1516-duwe-datenreduktion.pdf](https://hps.vi4io.org/_media/teaching/wintersemester_2015_2016/pre-1516-duwe-datenreduktion.pdf), 2016.
- [23] G. Mini, “Digital Pulse Processing for Physics Applications.” [https://agenda.infn.it/event/4307/contributions/51760/attachments/36739/43255/DPP\\_for\\_Physics\\_Application\\_Vulcano.pdf](https://agenda.infn.it/event/4307/contributions/51760/attachments/36739/43255/DPP_for_Physics_Application_Vulcano.pdf), 2012.
- [24] “ZeroMQ.” <https://zeromq.org/>.
- [25] DARKSIDE 20K collaboration, *Sensitivity of future liquid argon dark matter search experiments to core-collapse supernova neutrinos*, *JCAP* **03** (2021) 043 [2011.07819].

[26] W.O. Documentation, “WinCC OA Documentation.”  
[https://www.winccoa.com/documentation/WinCCOA/latest/en\\_US/index.html](https://www.winccoa.com/documentation/WinCCOA/latest/en_US/index.html).